Biomolecules and Biomedicine
ISSN: 2831-0896 (Print) | ISSN: 2831-090X (Online)
Journal Impact Factor® (2024): 2.2
CiteScore® (2024): 5.2
www.biomolbiomed.com

RESEARCH ARTICLE

Johnson et al: Decitabine, MMTV and IFN-β in tumors

Decitabine suppresses tumor growth by activating mouse mammary tumor virus and interferon-β pathways

Ryan Johnson, Andrew Brola, Cade Wycoff, William Wycoff, Seth Neumeyer, Richard Tuttle, Sarah Light, Jiayi Li, Stephen Christensen, Yingguang Liu*

Department of Biomedical Sciences, College of Osteopathic Medicine, Liberty University, Lynchburg, VA

*Correspondence to Yingguang Liu: yliu@liberty.edu

DOI: https://doi.org/10.17305/bb.2025.12852

ABSTRACT

Decitabine (DAC), a DNA methyltransferase inhibitor (DNMTi), is clinically effective in hematological malignancies such as myelodysplastic syndrome and acute myeloid leukemia, but its precise antineoplastic mechanisms remain incompletely understood. Beyond promoter demethylation, DAC is known to activate endogenous retroviruses (ERVs) and trigger type I interferon (IFN-I) responses, a phenomenon known as viral mimicry. The aim of this study was to investigate the roles of the mouse mammary tumor virus (MMTV) and interferon-β (IFN-β) in DAC-mediated tumor suppression. We employed two murine tumor models—4T1 mammary carcinoma and MC38 colon adenocarcinoma—in syngeneic immunocompetent mice, immunodeficient nude mice, and *in vitro* cultures. RNA and protein expression were assessed by quantitative PCR and immunoblotting, while functional contributions of MMTV and IFN-β were tested using short hairpin RNA (shRNA) knockdowns. DAC treatment suppressed tumor growth and pulmonary metastasis *in vivo* and inhibited cancer cell proliferation *in vitro*. It induced transcription of MMTV and expression of IFN-β, with a strong negative correlation between MMTV Env protein levels and tumor mass. Knockdown of either MMTV or IFN-β conferred resistance to DAC, confirming their functional roles. Reciprocal regulation was observed: MMTV knockdown reduced IFN-β expression, while IFN-β knockdown increased MMTV Env accumulation. Furthermore, DAC upregulated interferon regulatory factor 7 (IRF7), but this effect declined during prolonged treatment, suggesting a temporally restricted therapeutic window. In conclusion, our findings provide *in vivo* support for the viral mimicry hypothesis and demonstrate that MMTV and IFN-β contribute to DAC-mediated tumor suppression. The observed IRF7 downregulation and potential induction of immune checkpoints highlight the importance of therapeutic strategies combining DNMTis with immune checkpoint blockade to sustain antineoplastic efficacy.

Keywords: Decitabine, DNA methyltransferase inhibitor, mouse mammary tumor virus, interferon, tumor, cancer, 4T1, MC38, interferon regulatory factor 7.

INTRODUCTION

DNA methyltransferase inhibitors (DNMTis), such as azacitidine (AZA) and decitabine (DAC), are effective in the treatment of certain hematological cancers, including myelodysplastic syndrome (MDS) and acute myeloid leukemia (AML). However, their mechanisms of action remain poorly understood. Even though the drugs are known to alter the expression of hundreds of genes by demethylating their promoters [1,2], researchers found no drug-specific DNA methylation pattern or canonical target genes altered by DAC in AML cells [3]. There are indications that hypomethylation reactivates tumor-suppressor genes and induces apoptosis, but the exact mode of action of DNMTis in patients remains ill-defined [4,5].

Beyond the direct effect of DNA hypomethylation on cell proliferation and apoptosis, DNMTis are known to modulate the immunological environment in cancer patients and tumor-bearing mice [6]. Specifically, DAC has been shown to suppress the expansion and function of myeloid derived suppressor cells (MDSCs), activate $CD4^+$ T cells, enhance the expression of MHC molecules and tumor-specific antigens, thus synergizing with cytotoxic T lymphocytes [7, 8, 9, 10]. In addition, DNMTis activate the expression of endogenous retroviruses (ERVs), which in turn induce antineoplastic type I interferons (IFN-I), leading to the viral mimicry hypothesis [11]. Sensors of double-stranded RNA (dsRNA) involved in the interferon response include Toll-like receptor 3, mitochondrial antiviral-signaling protein (MAVS), and Staufen1. Interferon regulatory factor 3 and a long noncoding RNA called TINCR also play roles in the process [11, 12]. The viral mimicry effect of DNMTis has led to a renewed interest in interferon-oriented cancer therapies and the mechanisms of interferon regulation in the cancer microenvironment [13]. However, most of the evidence supporting the viral mimicry hypothesis has been derived *in vitro,* and there is a dearth of *in vivo* mechanistic studies.

The goal of this study was to investigate DAC-induced viral mimicry in murine tumor models. We used two murine tumor cell lines: 4T1, a mouse mammary tumor cell line derived from the BALB/c strain, and a colon adenocarcinoma cell line, MC38, derived from C57BL/6 mice. Both cell lines readily form solid tumors in their syngeneic host strains. The genomes of these cell lines harbor endogenous proviruses of the mouse

mammary tumor virus (MMTV, or *Mtv* for endogenous versions), which can be transmitted both endogenously by Mendelian inheritance and exogenously via milk [14]. MMTV is a major driver of mouse mammary tumors [15]. We studied the roles of MMTV and interferon-β (IFN-β) in the antineoplastic action of DAC and found that DAC treatment activates MMTV expression, which, in turn, induces IFN-β expression in tumor cells, ultimately leading to decelerated cell proliferation and delayed tumor growth. Notably, we also observed a rapid initial upregulation of interferon regulatory factor 7 (IRF7) which gradually declined over the course of DAC treatment.

MATERIALS AND METHODS

Cell lines, culturing, and *in vitro* drug treatment

The 4T1 murine mammary cancer cell line (American Type Culture Collection; with STR authentication) was maintained in RPMI 1640 with 10% fetal bovine serum (FBS). The MC38 cell line (kindly provided by Dr. Anthony Bauer, STR authenticated) was maintained in Dulbecco's Modified Eagle Medium (DMEM) with 10% FBS. All cells were cultured at 37˚C with 5% CO_2. DAC (MedChemExpress) was dissolved in dimethyl sulfoxide (DMSO) and added to the culture media to 100 nM. Recombinant mouse interferon-α2 (VWR) was dissolved in water and added to culture media at 2 ng/mL and 20 ng/mL. After 3-4 days of treatment, cells were trypsinized and counted using a NucleoCounter NC-3000 (Chemometec) according to the manufacturer's instructions. Cell lines were treated with BM-Cyclin to eliminate potential mycoplasma infection.

Extraction of RNA, reverse transcription, and quantitative PCR

RNA extraction, reverse transcription, real-time PCR, as well as the primers for MMTV and the *PGK1* reference gene, were the same as described in [16]. (We compared multiple housekeeping genes in the Mouse Housekeeping Gene Primer Set from RealTimePrimers using the NormFinder algorithm [17] and found *pGK1* being most stable). Primers for the *IFNB1* gene (RealTimePrimers.com), which encodes IFN-β, were used at 200 nM. The annealing temperature for *IFNB1* was 61°C. All samples were quantified in triplicate wells. All quantities were calculated using the ΔΔCt method. All primer pairs had amplification efficiencies above 90%, producing a single band upon agarose gel electrophoresis and a single peak in melting point analyses.

Plasmids, lentiviral packaging and transduction

MMTV shRNA plasmids were custom designed and constructed by OriGene. Two of them targeted the *env* gene. KD1 targeted nucleotides 6394-6422 according to GenBank AF033807.1, while KD3 targeted 6720-6748. KD2 targeted the *pol* gene (5186-5214). Mouse *IFNB1* shRNA plasmids were purchased from OriGene. In both cases, 29-mer shRNA constructs were expressed with the pGFP-C-ShLenti lentiviral vector. For the control, the same vector was used to express scrambled 29-mer shRNA. Lentiviral packaging and transduction were the same as in [16]. To select transduced 4T1 cells, the puromycin concentration was gradually increased from 0.5 μg/mL to 10 μg/mL.

Immunoblotting

Immunoblotting was performed as described in [16]. Tissue or cultured cells were lysed in RIPA buffer. The Invitrogen iBlot 2 Gel Transfer Device was used for transfer onto PVDF membranes. Polyclonal rabbit anti-MMTV Env (Bosterbio A30410) was used at 1:2000. Polyclonal rabbit anti-IFNB (MyBioSource MBS9607127) was used at 1:3000. Polyclonal rabbit anti-IRF7 was used at 1:1000. Monoclonal mouse anti-GAPDH (Bosterbio M00227-6) was used at 1:3000. All primary antibodies were incubated overnight at 4°C. HRP-conjugated goat anti-rabbit IgG (Bosterbio) and IRDye800CW-labelled donkey-anti-mouse (LI-COR) were used at 1:10,000. Reactions with the secondary antibodies were carried out at room temperature for 1 hour. Enhanced chemiluminescence (Bosterbio) and infrared fluorescence were photographed using the ChemiDoc MP (Bio-Rad) or scanned with the Odyssey CLx Infrared Imaging System (Li-Cor). Image Studio (Li-Cor) and Image Lab (Bio-Rad) software was used to quantify band intensities. Target protein quantities were normalized against that of GAPDH to generate densitograms.

Mouse models

Female BALB/c, C57BL/6, or NU/J mice (7-8 weeks old with body weights at 19.2±1.6 g, 18.7±1.0 g, and 23.8±1.4 g respectively) were inoculated with 30,000 4T1 cells or 200,000 MC38 cells suspended in 50-100 μL of Versene solution (ThermoFisher), subcutaneously, using a 30½-gauge needle under nipple number 4. After the tumors were palpable (typically ~1 week after inoculation), the mice were divided into treatment

groups using the minimization method according to tumor size and body weight [18]. DAC was administered by subcutaneous injection every other day at 0.42 mg/Kg for BALB/c mice and NU/J mice (except for the MMTV knockdown experiment where DAC was used at 0.78 mg/Kg), and 0.53 mg/Kg for C57BL/6 mice. The drug was dissolved in DMSO, frozen in -80°C, and diluted 100-fold in phosphate-buffered saline (PBS) for subcutaneous injection on the back. Control mice received the same volume of PBS with 1% DMSO. Mice were weighed twice a week. The volume of tumors was calculated as 0.5 x length x width^2. Experiments were terminated before tumors reached 20% of body weight or when mice showed signs of being moribund. Tumor mass was weighed after the mice were euthanized. Metastatic colony count was performed as described [16]. The students who measured tumors and counted the colonies were unaware of the group allocation while performing the measurements and counting. Mouse use was approved by the Institutional Animal Care and Use Committee of Liberty University (protocol numbers 70, 75, 81, 89, 96, 98).

Statistical analysis

The two-tailed exact Mann-Whitney U test was used to compare two sets of quantitative data. When multiple groups were studied, pairwise comparisons were preplanned. Statistical significance was called at $p < 0.05$. Correlation coefficients were calculated and tested with the Spearman's Rho Calculator [19]. Two-tailed post hoc power analysis was performed using G*Power with Cohen's d for effect sizes [20].

RESULTS

DAC inhibited tumor growth and metastasis in both immunocompetent mice and nude mice

We inoculated both 4T1 cells and MC38 cells in the subcutaneous tissue of the corresponding syngeneic mice (BALB/c and C57B/6, respectively) and nude mice under nipple number 4. After tumors became palpable, DAC was administered every other day via subcutaneous injection for 3-4 weeks. Pulmonary metastasis of 4T1 tumors was evaluated by colony count in cell cultures after the mice were sacrificed.

DAC effectively inhibited the overall growth of both 4T1 and MC38 tumors in syngeneic mice as well as in nude mice (Figure 1A-1C). However, the rate of primary tumor growth

subsequently accelerated after 2-3 weeks of DAC treatment. DAC also inhibited pulmonary metastasis of the 4T1 tumor in both BALB/c mice and nude mice (Figure 1D).

DAC enhanced expression of MMTV which is correlated with tumor suppression

DAC treatment of mice enhanced the RNA expression of the *env* and *pol* genes of MMTV in both 4T1 and MC38 tumors as determined by qRT-PCR (Figure 1E-F). Expression of the MMTV Env protein varied in both treated and untreated mice. A 70-80-kDa Env precursor was detected in both groups but demonstrated greater intensity in DAC-treated tumors, while a 40-45-kDa band was prominent only in the treated group (Figure 1G). Importantly, there was a significant negative correlation between Env quantity and tumor mass, with a Spearman correlation coefficient of -0.88 (Figure 1H).

MMTV knockdown conferred resistance to DAC

To investigate the role of MMTV in DAC-mediated tumor suppression, we constructed shRNA-expressing lentiviral plasmids targeting MMTV *env* and *pol* genes and transduced them into 4T1 cells. Knockdown of MMTV rendered 4T1 cells more resistant to DAC *in vitro* as shown in the higher number of surviving cells in the presence of DAC compared with control (viable cell counts with the NucleoCounter) (Figure 2A and 2B) and *in vivo* (Figure 2C and 2D). Among the knockdown cell lines, MMTV knockdown was more efficient in KD1 than in KD3. (See Table 1 for knockdown efficiencies. KD2 was not used due to low efficiency.) Correspondingly, the KD1 tumors experienced greater resistance to DAC (Figure 2C and 2D).

To further characterize the involvement of MMTV in DAC treatment, we quantified *env* and *pol* transcripts in knockdown cell lines in the presence and absence of DAC (Figure 2E and 2F). RNA expression of *env* and *pol* was significantly reduced in knockdown cell lines relative to controls. Importantly, DAC-induced upregulation of MMTV transcription was restricted in knockdown cells.

DAC upregulated expression of IFN-β in tumor cells

DAC treatment enhanced the expression of IFN-β in the mouse tumor cell lines on both the RNA and protein levels (Figure 3A and 3B). This was accompanied by increased expression of IRF7, which rose rapidly following DAC treatment but gradually declined over the course of treatment (Figure 3B). A Mann-Kendall test confirms the declining

trend of IRF7 protein level from day 2 to day 15 with 96% confidence. Furthermore, knockdown of MMTV in 4T1 cells resulted in a corresponding decrease in IFN-β expression (Figure 3C), while knockdown of IFN-β led to an accumulation of MMTV Env (Figure 3D). These findings highlight a critical reciprocal relationship between MMTV and IFN-β expression.

IFN-β knockdown conferred resistance to DAC

Lentiviral plasmids expressing shRNA to target different splice variants of the *IFNB1* gene were used to knock down *IFNB1* in 4T1 cells (See Table 1 for knockdown efficiencies of KD1 and KD2 cell lines which were used in subsequent experiments). Knocking down IFN-β rendered 4T1 cells more resistant to DAC *in vitro* and *in vivo* (Figure 3F-I). Interestingly, untreated KD1 tumors grew faster than untreated control tumors, consistent with a tumor-suppressive role of IFN-β. To confirm that the accelerated growth of KD1 was due to knockdown of an IFN-I, we treated control and knockdown cell lines *in vitro* with recombinant interferon-α2 (IFN-α2). Growth of both knockdown cell lines slowed down significantly in the presence of low concentrations of IFN-α2 while the control cell line was unaffected (Figure 3E). Evidently, *IFNB1* knockdown enhanced sensitivity of the 4T1 cells to exogenous IFN-α2. The slower growth of KD2 was likely due to the off-target effect of lentiviral insertions.

DISCUSSION

To our knowledge, this is the first study of the viral mimicry hypothesis in murine tumor models. Our findings demonstrate that DAC suppresses murine tumor growth and metastasis, an effect that is at least partially mediated by MMTV and IFN-β.

Role of viral RNA and proteins

Expression of viral RNA, especially dsRNA, can trigger an antiviral response through interferon signaling [21]. Consistent with previous findings with human ERVs [11], DAC treatment induced more pronounced increases in MMTV RNA transcription than MMTV protein production. This discrepancy between RNA transcripts and protein production is presumably a result of interferon-stimulated genes such as the Zinc Finger Antiviral Protein (ZAP) and RNA-activated protein kinase (PKR) that inhibit retroviral translation [22]. However, we observed a correlation between MMTV Env protein quantity and the

antineoplastic effect of DAC. This suggests that MMTV protein may contribute to tumor suppression as a neoantigen [9].

Role of IFN-β in controlling viruses and tumors

While IFN-α and IFN-γ are mostly produced by professional immune cells, IFN-β is produced by most nucleated cells during a viral infection. We revealed in this study that IFN-β knockdown led to accumulation of the MMTV Env protein, supporting an antiviral role of IFN-β. IFN-β also appears to inhibit tumor growth even in the absence of DAC stimulation as one of the IFN-β knockdown cell lines (KD1) established faster growing tumors than control cells.

The relationship between IFN-β and IRF7

Upregulation of IRF7 expression has been recently reported in DAC-treated cell cultures and in tumor tissues of DAC-treated patients [23,24], and our findings corroborate these reports. Mice are known to express high levels of IRF7 that upregulates the production of multiple proinflammatory cytokines [25]. IRF7 is a key transcription factor that mediates the downstream effects of pattern-recognition receptor signaling, leading to the production of IFN-I [24, 26]. Interestingly, IFN-I also activate IRF7 expression through the JAK-STAT pathway, forming a positive feedback loop [27-29]. In accordance with this mutual stimulation, we observed a concurrent increase of IFN-β and IRF7 in DAC treated cells and tumors. Because IRF7 is expressed by many cell types in the tumor microenvironment, including plasmacytoid dendritic cells, monocytes, B cells, and fibroblasts [29-31], the tumor mesenchyme likely contributes to this positive feedback loop.

Downregulation of interferon response in prolonged treatment

The observed subsequent downregulation of IRF7 during continued DAC therapy may help explain the diminished effects of DAC after several weeks of treatment (Figure 1A, 2C, and 3H). There are several potential mechanisms that suppress responses to IFN-I, including downregulation of the interferon receptor (IFNAR), induction of negative regulators, and the induction of miRNAs [32]. There are also molecules that potently downregulate IRF7. For example, both IFN-I and IRF7 induce the expression of the activating transcription factor 4 (ATF4) which, in turn, binds IRF7 to inactivate it [33]

(Figure 4). IFN-I also induce the suppressor of cytokine signaling (SOCS) proteins to promote the degradation of IRF7 [34]. While modulation of interferon responses serves to prevent interferon-mediated autoimmunity, it may also undermine the efficacy of DAC therapy and other cancer therapies that rely on intact interferon responses. Conversely, in the *IFNB1* knockdown cell lines, the interferon response system including the IFNAR may be upregulated in compensation, explaining their enhanced sensitivity to exogenous IFN-α (Figure 3E).

DAC, interferons, and T cells

IFN-I inhibit tumor growth through direct antiproliferative effects and immunomodulatory effects. Mechanistically, interferons downregulate oncogene expression, induce tumor suppressor genes, promote tumor cell apoptosis, enhance expression of MHC molecules, inhibit angiogenesis, activate T lymphocytes and natural killer cells, stimulate dendritic cells, and other tumor suppressive functions [35]. The fact that DAC is no less effective in nude mice than in immunocompetent mice indicates that T lymphocytes do not play a major role in its mechanisms of action. However, synergy between DAC treatment and adoptive T cell immunotherapy in mice suggests a T cell-activating effect of DAC in immunocompetent hosts [7].

Other transposable elements and direct upregulation of IFN

Beyond ERVs, DAC activates other transposable elements such as LINE-1 in human cells [36]. It also directly demethylates the promoter of the *IFNB1* gene [37]. Such mechanisms likely exist in murine cancer cells, but the significant reduction of intracellular IFN-β with MMTV knockdown (Figure 3C) underlines the importance of MMTV in the regulation of IFN in the 4T1 cell line.

The paradoxical role of endogenous retroviruses in cancer

MMTV has homologues in the human genome, i.e., the human endogenous retrovirus type K (HERV-K) family, although the latter are more degraded and incapable of horizonal transmission [38]. Driven by sex hormones, HERV-Ks are upregulated in breast cancer cells [39], and their expression level is positively correlated with disease progression and unfavorable prognosis [40]. Therefore, the antineoplastic action of decitabine by stimulating ERV expression seems paradoxical. The answer may lie in

negative feedback and immune checkpoint control (Figure 4). DNMTi-activated viral mimicry leads to the production of antineoplastic IFN-I. However, virus-induced interferon production only lasts for a very brief time due to negative feedback [41]. Although decitabine stimulation of interferon production may last for a longer time because of the direct demethylation of the IRF7 promoter [24], chronic production of interferons in cancer patients can induce immune checkpoint molecules such as PD-L1 [42]. Once the interferon system is exhausted and/or the patient becomes immunotolerant, the tumor-promoting properties of ERVs gain dominance. It is also likely that high levels of ERV expression and tumor progression are both results of immunotolerance. For this reason, combining interferon-based therapy with immune checkpoint blockade has shown promising results [43], and the same approach may apply to DNA methyltransferase inhibitors [44].

Limitations of the study

Some of the quantitative analyses are underpowered to reveal statistical differences due to small sample sizes (Table 2). DAC likely elevates MMTV *pol* gene expression in 4T1 cells just like in MC38 cells, but the former did not reach statistical significance (Fig 1E-F). Likewise, 4T1 cells with MMTV knockdown (KD1) probably retain a degree of sensitivity to DAC *in vitro* just like *in vivo*, and the discrepancy between Fig 2A and Fig 2D is likely due to the smaller *in vitro* sample size and the shorter duration of *in vitro* treatment (3 days *in vitro* versus 4 weeks *in vivo*). On the other hand, statistical differences revealed by low power experiments indicate large effect sizes.

CONCLUSION

In agreement with the viral mimicry hypothesis, our studies demonstrate the involvement of the mouse mammary tumor virus and interferon-β in mediating the antineoplastic action of decitabine. There is also an upregulation of IRF7 by decitabine in the murine model. A subsequent decline in IRF7 expression suggests negative feedback in the action of interferon-β and provides an explanation for the eventual failure of decitabine in cancer treatment. Because interferons are known to activate immune checkpoint control, this study strengthens the theoretical basis for combining DNA methyltransferase inhibitors with immune checkpoint blockers.

Conflicts of interest: Authors declare no conflicts of interest.

Funding: The project was supported by intramural grants from the Liberty University College of Osteopathic Medicine.

Submitted: June 25, 2025

Accepted: August 16, 2025

Published online: August 27, 2025

REFERENCES

1. Bohl SR, Claus R, Dolnik A, Schlenk RF, Döhner K, Hackanson B, et al. Decitabine response associated gene expression patterns in acute myeloid leukemia (AML). Blood 2013;122(21): 3756. https://doi.org/10.1182/blood.V122.21.3756.3756.
2. Yan P, Frankhouser D, Murphy M, Tam HH, Rodriguez B, Curfman J, et al. Genome-wide methylation profiling in decitabine-treated patients with acute myeloid leukemia. Blood 2012;120(12):2466-74. https://doi.org/10.1182/blood-2012-05-429175.
3. Klco JM, Spencer DH, Lamprecht TL, Sarkaria SM, Wylie T, Magrini V, et al. Genomic impact of transient low-dose decitabine treatment on primary AML cells. Blood 2013;121(9):1633-43. https://doi.org/10.1182/blood-2012-09-459313.
4. Stresemann C, Lyko F. Modes of action of the DNA methyltransferase inhibitors azacytidine and decitabine. Int J Cancer 2008;123(1):8-13. https://doi.org/10.1002/ijc.23607.
5. Mpakou V, Spathis A, Bouhla A, Mpazani E, Papageorgiou S, Gkontopoulos K, et al. Synergistic inhibitory effects of low-dose decitabine in combination with bortezomib in the AML cell line Kasumi-1. Exp Ther Med 2021;21(3):195. https://doi.org/10.3892/etm.2021.9628.
6. Vatapalli R, Rossi AP, Chan HM, Zhang J. Cancer epigenetic therapy: recent advances, challenges, and emerging opportunities. Epigenomics 2025;17(1):59-74. https://doi.org/10.1080/17501911.2024.2430169.
7. Terracina KP, Graham LJ, Payne KK, Manjili MH, Baek A, Damle SR, et al. DNA methyltransferase inhibition increases efficacy of adoptive cellular immunotherapy of murine breast cancer. Cancer Immunol Immunother 2016;65(9):1061-73. https://doi.org/10.1007/s00262-016-1868-8.
8. Li X, Dong L, Liu J, Wang C, Zhang Y, Mei Q, et al. Low-dose decitabine augments the activation and anti-tumor immune response of IFN-γ^+ $CD4^+$ T cells through enhancing IκBα degradation and NF-κB activation. Front Cell Dev Biol 2021;9:647713. https://doi.org/10.3389/fcell.2021.647713.

9. Ma R, Rei M, Woodhouse I, Ferris K, Kirschner S, Chandran A, et al. Decitabine increases neoantigen and cancer testis antigen expression to enhance T-cell-mediated toxicity against glioblastoma. Neuro Oncol 2022;24(12):2093-2106. https://doi.org/10.1093/neuonc/noac107.
10. Zhang Z, Wang T, Fang G, Xiao X, Zhang Z, Zhao J. Decitabine suppresses MDSC-induced immunosuppression through dual functional mechanism and inhibits melanoma metastasis. Med Oncol 2024;41(7):165. https://doi.org/10.1007/s12032-024-02320-w.
11. Chiappinelli KB, Strissel PL, Desrichard A, Li H, Henke C, Akman B, Hein A, et al. Inhibiting DNA methylation causes an interferon response in cancer via dsRNA including endogenous retroviruses. Cell 2015;162(5):974-86. Erratum in: Cell 2016;164(5):1073. Erratum in: Cell 2017;169(2):361. https://doi.org/10.1016/j.cell.2015.07.011.
12. Ku Y, Park JH, Cho R, Lee Y, Park HM, Kim M, et al. Noncanonical immune response to the inhibition of DNA methylation by Staufen1 via stabilization of endogenous retrovirus RNAs. Proc Natl Acad Sci U S A 2021;118(13):e2016289118. https://doi.org/10.1073/pnas.2016289118.
13. Yu R, Zhu B, Chen D. Type I interferon-mediated tumor immunity and its role in immunotherapy. Cell Mol Life Sci. 2022;79(3):191. https://doi.org/10.1007/s00018-022-04219-z.
14. Ross SR. Mouse mammary tumor virus molecular biology and oncogenesis. Viruses 2010;2(9):2000-2012. https://doi.org/10.3390/v2092000.
15. Hook LM, Agafonova Y, Ross SR, Turner SJ, Golovkina TV. Genetics of mouse mammary tumor virus-induced mammary tumors: linkage of tumor induction to the gag gene. J Virol 2000;74(19):8876-83. https://doi.org/10.1128/jvi.74.19.8876-8883.2000.
16. Li J, Lin J, Lin JR, Farris M, Robbins L, Andrada L, et al. Dolutegravir inhibits proliferation and motility of BT-20 tumor cells through inhibition of human endogenous retrovirus type K. Cureus 2022;14(7):e26525. https://doi.org/10.7759/cureus.26525.

17. MOMA - Department of Molecular Medicine, Aarhus University Hospital and Aarhus University [Internet]. Aarhus N, Denmark: MOMA; 2025. NormFinder software; 2025 [cited 2025 July 13]. Available from: https://www.moma.dk/software/normfinder
18. Scott NW, McPherson GC, Ramsay CR, Campbell MK. The method of minimization for allocation to clinical trials. a review. Control Clin Trials. 2002 Dec;23(6):662-74. http://doi.org/10.1016/s0197-2456(02)00242-8.
19. Social Science Statistics [internet]. Jeremy Stangroom; c2018-2025. Spearman's Rho Calculator; 2018 [Cited 2025 May 13]. Available from: https://www.socscistatistics.com/tests/spearman/default.aspx
20. The G*Power Team. G*Power: Statistical Power Analyses for Mac and Windows [internet]. Düsseldorf: Heinrich-Heine-Universität Düsseldorf; 2025 [Cited 2025 July 31]. Available from: https://www.psychologie.hhu.de/arbeitsgruppen/allgemeine-psychologie-und-arbeitspsychologie/gpower.
21. Nagarajan U. Induction and function of IFNβ during viral and bacterial infection. Crit Rev Immunol 2011;31(6):459-74. https://doi.org/10.1615/critrevimmunol.v31.i6.20.
22. Jäger N, Pöhlmann S, Rodnina MV, Ayyub SA. Interferon-stimulated genes that target retrovirus translation. Viruses 2024;16(6):933. https://doi.org/10.3390/v16060933.
23. Roulois D, Loo Yau H, Singhania R, Wang Y, Danesh A, Shen SY, et al. DNA-Demethylating agents target colorectal cancer cells by inducing viral mimicry by endogenous transcripts. Cell 2015;162(5):961-73. https://doi.org/10.1016/j.cell.2015.07.056.
24. Wang H, Wang Z, Wang Z, Li X, Li Y, Yan N, et al. Decitabine induces IRF7-mediated immune responses in p53-mutated triple-negative breast cancer: a clinical and translational study. Front Med 2024;18(2):357-374. https://doi.org/10.1007/s11684-023-1016-8.

25. Chen Z, Gu Q, Chen R. Promotive role of IRF7 in ferroptosis of colonic epithelial cells in ulcerative colitis by the miR-375-3p/SLC11A2 axis. Biomol Biomed 2023;23(3):437-449. https://doi.org/10.17305/bjbms.2022.8081.
26. Zhou Q, Lavorgna A, Bowman M, Hiscott J, Harhaj EW. Aryl Hydrocarbon Receptor Interacting Protein Targets IRF7 to Suppress Antiviral Signaling and the Induction of Type I Interferon. J Biol Chem 2015;290(23):14729-39. https://doi.org/10.1074/jbc.m114.633065.
27. Marié I, Durbin JE, Levy DE. Differential viral induction of distinct interferon-alpha genes by positive feedback through interferon regulatory factor-7. EMBO J 1998;17(22):6660-9. https://doi.org/10.1093/emboj/17.22.6660.
28. Sato M, Hata N, Asagiri M, Nakaya T, Taniguchi T, Tanaka N. Positive feedback regulation of type I IFN genes by the IFN-inducible transcription factor IRF-7. FEBS Lett 1998;441(1):106-10. https://doi.org/10.1016/s0014-5793(98)01514-2.
29. Qing F, Liu Z. Interferon regulatory factor 7 in inflammation, cancer and infection. Front Immunol 2023;14:1190841. https://doi.org/10.3389/fimmu.2023.1190841.
30. Honda K, Yanai H, Negishi H, Asagiri M, Sato M, Mizutani T, *et al.* IRF-7 is the master regulator of type-I interferon-dependent immune responses. Nature 2005; 434:772–777. https://doi.org/10.1038/nature03464.
31. Ning S, Pagano JS, Barber GN. IRF7: activation, regulation, modification and function. Genes Immun 2011;12(6):399-414. https://doi.org/10.1038/gene.2011.21.
32. Ivashkiv LB, Donlin LT. Regulation of type I interferon responses. Nat Rev Immunol 2014;14(1):36-49. https://doi.org/10.1038/nri3581.
33. Liang Q, Deng H, Sun CW, Townes TM, Zhu F. Negative regulation of IRF7 activation by activating transcription factor 4 suggests a cross-regulation between the IFN responses and the cellular integrated stress responses. J Immunol 2011 Jan 15;186(2):1001-10. https://doi.org/10.4049/jimmunol.1002240.

34. Yu CF, Peng WM, Schlee M, Barchet W, Eis-Hübinger AM, Kolanus W, et al. SOCS1 and SOCS3 target IRF7 degradation to suppress TLR7-mediated type I IFN production of human plasmacytoid dendritic cells. J Immunol 2018;200(12):4024-4035. https://doi.org/10.4049/jimmunol.1700510.
35. Ferrantini M, Capone I, Belardelli F. Interferon-alpha and cancer: mechanisms of action and new perspectives of clinical use. Biochimie 2007;89(6-7):884-93. https://doi.org/10.1016/j.biochi.2007.04.006.
36. de Cubas AA, Dunker W, Zaninovich A, Hongo RA, Bhatia A, Panda A, et al. DNA hypomethylation promotes transposable element expression and activation of immune signaling in renal cell cancer. JCI Insight 2020;5(11):e137569. https://doi.org/10.1172/jci.insight.137569.
37. Wu J, Li Y, Wu J, Song H, Tang Y, Yan N, et al. Decitabine activates type I interferon signaling to inhibit p53-deficient myeloid malignant cells. Clin Transl Med 2021;11(11):e593. https://doi.org/10.1002/ctm2.593.
38. Lee YN, Bieniasz PD. Reconstitution of an infectious human endogenous retrovirus. PLoS Pathog 2007; 3(1):e10. https://doi.org/10.1371/journal.ppat.0030010.
39. Nguyen TD, Davis J, Eugenio RA, Liu Y. Female Sex Hormones Activate Human Endogenous Retrovirus Type K Through the OCT4 Transcription Factor in T47D Breast Cancer Cells. AIDS Res Hum Retroviruses 2019;35(3):348-356. https://doi.org/10.1089/AID.2018.0173.
40. Zhao J, Rycaj K, Geng S, Li M, Plummer JB, Yin B, et al. Expression of Human Endogenous Retrovirus Type K Envelope Protein is a Novel Candidate Prognostic Marker for Human Breast Cancer. Genes Cancer 2011;2(9):914-22. https://10.1177/1947601911431841.
41. Greene TT, Zuniga EI. Type I Interferon Induction and Exhaustion during Viral Infection: Plasmacytoid Dendritic Cells and Emerging COVID-19 Findings. Viruses. 2021 Sep 15;13(9):1839. https://doi.org/10.3390/v13091839.
42. Morimoto Y, Kishida T, Kotani SI, Takayama K, Mazda O. Interferon-β signal may up-regulate PD-L1 expression through IRF9-dependent and independent

pathways in lung cancer cells. Biochem Biophys Res Commun 2018;507(1-4):330-336. https://doi.org/10.1016/j.bbrc.2018.11.035.

43. Razaghi A, Durand-Dubief M, Brusselaers N, Björnstedt M. Combining PD-1/PD-L1 blockade with type I interferon in cancer therapy. Front Immunol. 2023 Aug 24;14:1249330. http://doi.org/10.3389/fimmu.2023.1249330.
44. Chiappinelli KB, Zahnow CA, Ahuja N, Baylin SB. Combining Epigenetic and Immunotherapy to Combat Cancer. Cancer Res. 2016 Apr 1;76(7):1683-9. https://doi.org/10.1158/0008-5472.CAN-15-2125.

TABLES AND FIGURES WITH LEGENDS

Table 1. Knockdown efficiencies (percent reduction in mRNA and protein)

Cell line	mRNA	Protein
MMTV KD1	81.6	83
MMTV KD3	76	69.8
IFNB1 KD1	79.4	69.1
IFNB1 KD2	84.7	80.1

Abbreviations: MMTV, mouse mammary tumor virus; *IFNB1*, interferon beta 1; KD, knockdown (KD1, KD2, KD3 denote distinct knockdown lines); mRNA, messenger RNA.

Table 2. Post hoc calculation of achieved power for *in vitro* comparisons of knockdown cell lines

Figure	Power
2A for DAC treatment of control samples	0.94
2A for DAC treatment of KD1 samples	0.27
2B for percent inhibition difference	0.71
3E for control and KD1 cell growth	1
3E for IFN-α on KD1 at 2 ng/mL	0.91
3E for IFN-α on KD1 at 20 ng/mL	1
3E for IFN-α on KD2 at 2 ng/mL	0.34
3E for IFN-α on KD12 at 20 ng/mL	0.99
3F for DAC treatment of control samples	0.9
3G for percent inhibition differences	1

Abbreviations: DAC, decitabine (5-aza-2′-deoxycytidine); KD, knockdown (KD1, KD2 denote distinct knockdown lines); IFN-α, interferon alpha.

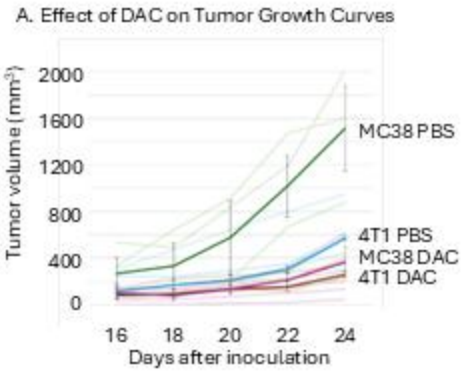
A. Effect of DAC on Tumor Growth Curves
Tumor volume (mm³)
2000
1600
1200
800
400
0
16
18
20
22
24
Days after inoculation
MC38 PBS
4T1 PBS
MC38 DAC
4T1 DAC

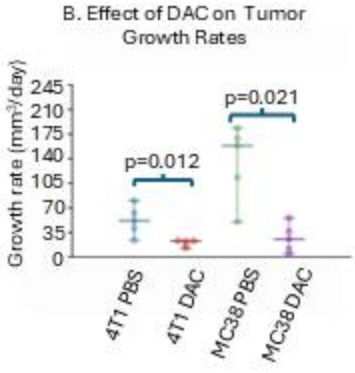
B. Effect of DAC on Tumor Growth Rates
Growth rate (mm³/day)
245
210
175
140
105
70
35
0
p=0.012
p=0.021
4T1 PBS
4T1 DAC
MC38 PBS
MC38 DAC

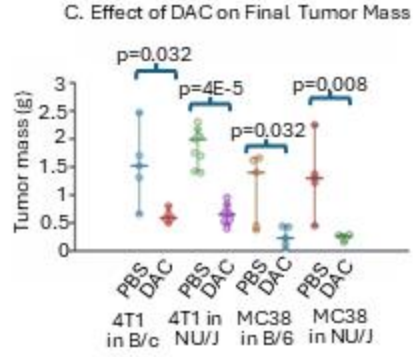
C. Effect of DAC on Final Tumor Mass
Tumor mass (g)
3
2.5
2
1.5
1
0.5
0
p=0.032
p=4E-5
p=0.032
p=0.008
PBS
DAC
4T1 in B/c
4T1 in NU/J
MC38 in B/6
MC38 in NU/J

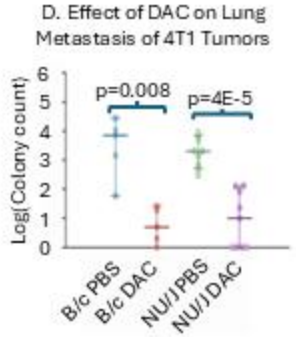
D. Effect of DAC on Lung Metastasis of 4T1 Tumors
Log(Colony count)
6
5
4
3
2
1
0
p=0.008
p=4E-5
B/c PBS
B/c DAC
NU/J PBS
NU/J DAC

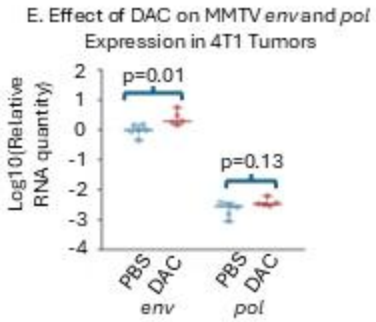
E. Effect of DAC on MMTV env and pol Expression in 4T1 Tumors
Log10(Relative RNA quantity)
2
1
0
-1
-2
-3
-4
p=0.01
p=0.13
PBS
DAC
env
pol

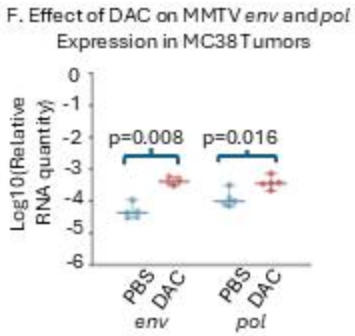
F. Effect of DAC on MMTV env and pol Expression in MC38 Tumors
Log10(Relative RNA quantity)
0
-1
-2
-3
-4
-5
-6
p=0.008
p=0.016
PBS
DAC
env
pol

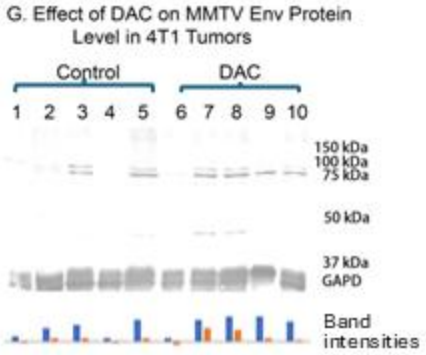
G. Effect of DAC on MMTV Env Protein Level in 4T1 Tumors
Control
DAC
1 2 3 4 5 6 7 8 9 10
150 kDa
100 kDa
75 kDa
50 kDa
37 kDa
GAPD
Band intensities

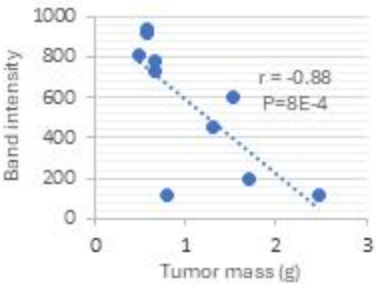
H. Correlation between 80-kDa Env signal strength and tumor mass
Band intensity
1000
800
600
400
200
0
r = -0.88
P=8E-4
0
1
2
3
Tumor mass (g)

Figure 1. DAC treatment, tumor growth/metastasis assessments, and MMTV expression readouts in murine tumor models. (A) Tumor growth curves for 4T1 (BALB/c) and MC38 (C57BL/6) tumors treated with decitabine (DAC) or vehicle (PBS); *n* = 5 mice per group. Individual trajectories are shown with group medians overlaid (x-axis: days after inoculation; y-axis: tumor volume, mm^3). (B) Tumor growth rates derived as linear-regression slopes of the curves in (A). Points indicate group medians with 95% CIs; p values are annotated. (C) Final tumor mass across strains and treatments: 4T1 in BALB/c and NU/J; MC38 in C57BL/6 and NU/J. *n* = 5 per group except 4T1 in NU/J (*n* = 9). Medians with 95% CIs. (D) Lung metastasis of 4T1 tumors quantified as log10 colony counts from lung cell cultures. *n* = 5 for BALB/c; *n* = 9 for NU/J. Medians with 95% CIs. (E) MMTV *env* and *pol* RNA in 4T1 tumors (BALB/c) measured by qRT-PCR and displayed as log10 relative quantity (PBS n = 6; DAC *n* = 5). (F) MMTV *env* and *pol* RNA in MC38 tumors (C57BL/6) measured by qRT-PCR (*n* = 5 per group). (G) Immunoblot of MMTV Env in 4T1 tumors: lanes 1–5 PBS; lanes 6–10 DAC. Bands near ~80 kDa and ~45 kDa are shown; GAPDH (37 kDa) is the loading control. Bar plot summarizes band intensities per lane. (H) Scatter plot of tumor mass versus Env band intensity for the 10 4T1 tumors in (G); five PBS and five DAC samples. Spearman correlation statistics are annotated in the panel.

Abbreviations: DAC, decitabine (5-aza-2′-deoxycytidine); PBS, phosphate-buffered saline; MMTV, mouse mammary tumor virus; *env/pol*, MMTV genes; qRT-PCR, quantitative reverse-transcription PCR; kDa, kilodalton; CI, confidence interval; BALB/c = B/c; C57BL/6 = B/6; NU/J, nude mice; *n*, number of mice.

A. Effect of MMTV Knockdown and DAC on 4T1 Cell Proliferation

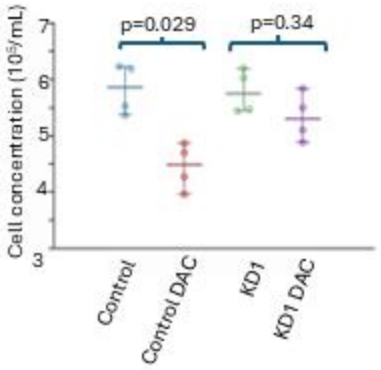

B. Effect of MMZTV Knockdown on DAC Sensitivity of 4T1 Cells *In Vitro*

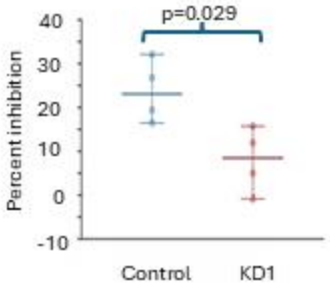

C. Effect of MMTV Knockdown and DAC on Growth Curves of 4T1 Tumors in BALB/c Mice

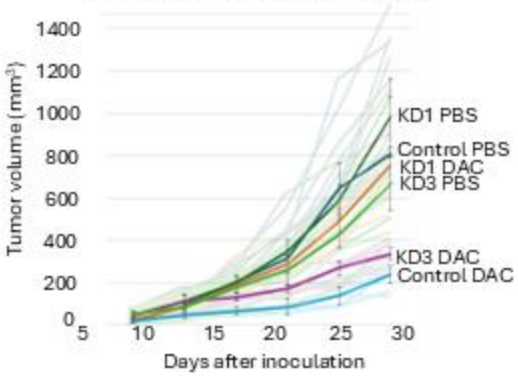

D. Effect of MMTV Knockdown and DAC on Growth Rates of 4T1 Tumors in BALB/c Mice

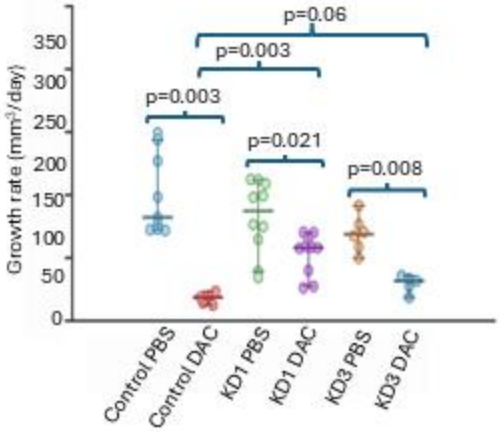

E. Effect of DAC on MMTV *env* Expression in Control and Knockdown Tumors

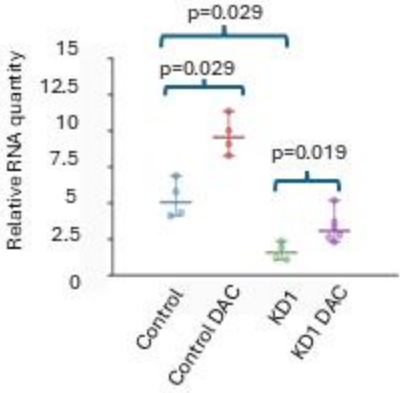

F. Effect of DAC on MMTV *pol* Expression in Control and Knockdown Tumors

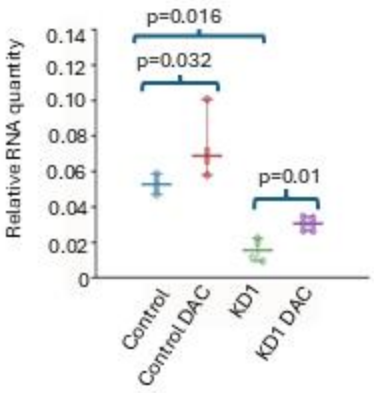

Figure 2. MMTV knockdown reduces sensitivity of 4T1 cells and tumors to DAC treatment. (A) Effect of MMTV knockdown and DAC treatment on proliferation of 4T1 cells. Cell viability was determined by NucleoCounter analysis after DAC exposure. (B) Effect of MMTV knockdown on DAC-mediated growth inhibition of 4T1 cells in vitro. Percent inhibition was calculated relative to untreated controls. (C) Impact of MMTV knockdown and DAC on tumor growth kinetics of 4T1 tumors in BALB/c mice. Tumor volumes were monitored over time following inoculation and treatment with PBS or DAC. (D) Growth rate analysis of 4T1 tumors in BALB/c mice after MMTV knockdown and DAC treatment. Pairwise comparisons were performed between PBS- and DAC-treated groups, as well as between control and knockdown tumors. (E) Quantification of MMTV *env* transcript levels in control and knockdown tumors with or without DAC treatment. Relative expression was determined by qRT-PCR. (F) Quantification of MMTV *pol* transcript levels in control and knockdown tumors with or without DAC treatment. Relative expression was determined by qRT-PCR.

Values represent group medians with 95% confidence intervals. $n = 4$ for in vitro assays (A–B); $n = 9$ for control tumors, $n = 10$ for KD1, and $n = 5$ for KD3 in in vivo experiments (C–D); $n = 4$–6 for transcript quantification (E–F). Abbreviations: MMTV, mouse mammary tumor virus; DAC, decitabine; PBS, phosphate-buffered saline; KD, knockdown; qRT-PCR, quantitative reverse transcription polymerase chain reaction.

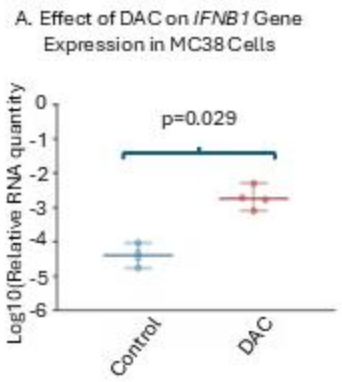
A. Effect of DAC on *IFNB1* Gene Expression in MC38 Cells
Log10(Relative RNA quantity
0
-1
-2
-3
-4
-5
-6
p=0.029
Control
DAC

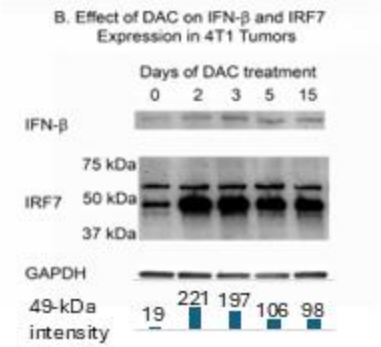
B. Effect of DAC on IFN-β and IRF7 Expression in 4T1 Tumors
Days of DAC treatment
0 2 3 5 15
IFN-β
75 kDa
IRF7 50 kDa
37 kDa
GAPDH
49-kDa intensity
19 221 197 106 98

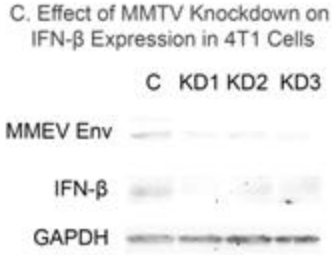
C. Effect of MMTV Knockdown on IFN-β Expression in 4T1 Cells
C KD1 KD2 KD3
MMEV Env
IFN-β
GAPDH

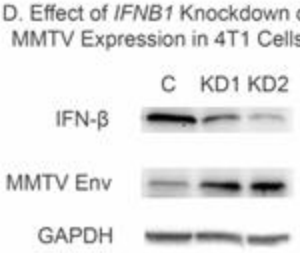
D. Effect of *IFNB1* Knockdown on MMTV Expression in 4T1 Cells
C KD1 KD2
IFN-β
MMTV Env
GAPDH

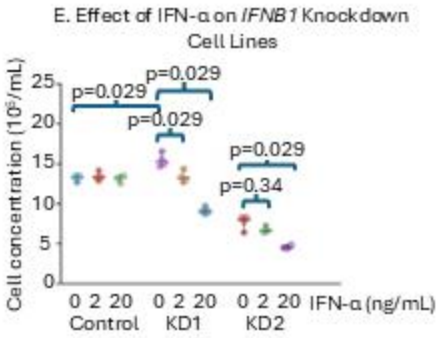
E. Effect of IFN-α on *IFNB1* Knockdown Cell Lines
Cell concentration (10⁵/mL)
25
20
15
10
5
0
p=0.029
p=0.029
p=0.029
p=0.029
p=0.34
0 2 20 0 2 20 0 2 20 IFN-α (ng/mL)
Control KD1 KD2

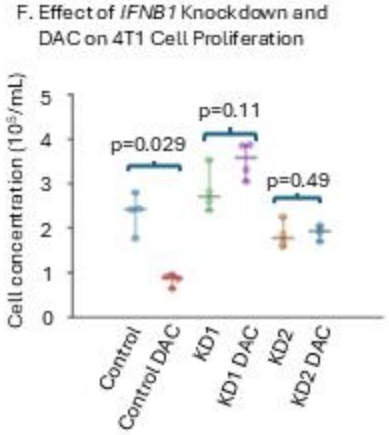
F. Effect of *IFNB1* Knockdown and DAC on 4T1 Cell Proliferation
Cell concentration (10⁵/mL)
5
4
3
2
1
0
p=0.029
p=0.11
p=0.49
Control
Control DAC
KD1
KD1 DAC
KD2
KD2 DAC

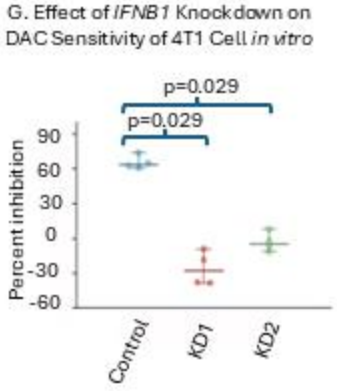
G. Effect of *IFNB1* Knockdown on DAC Sensitivity of 4T1 Cell *in vitro*
Percent inhibition
90
60
30
0
-30
-60
p=0.029
p=0.029
Control
KD1
KD2

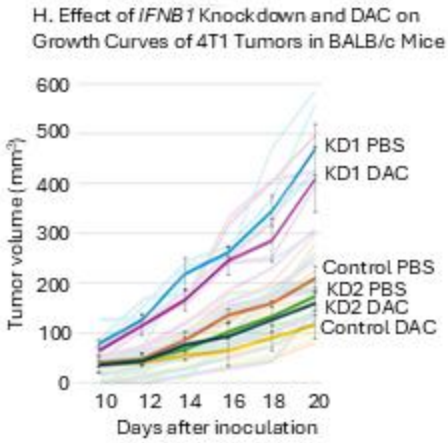
H. Effect of *IFNB1* Knockdown and DAC on Growth Curves of 4T1 Tumors in BALB/c Mice
Tumor volume (mm³)
600
500
400
300
200
100
0
10 12 14 16 18 20
Days after inoculation
KD1 PBS
KD1 DAC
Control PBS
KD2 PBS
KD2 DAC
Control DAC

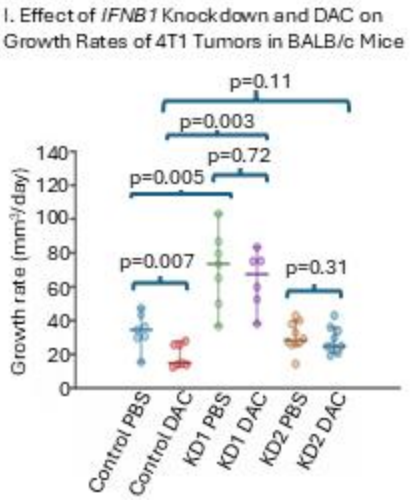
I. Effect of *IFNB1* Knockdown and DAC on Growth Rates of 4T1 Tumors in BALB/c Mice
Growth rate (mm³/day)
140
120
100
80
60
40
20
0
p=0.11
p=0.003
p=0.72
p=0.005
p=0.007
p=0.31
Control PBS
Control DAC
KD1 PBS
KD1 DAC
KD2 PBS
KD2 DAC

Figure 3. IFN-β mediates the antitumor effect of DAC and reciprocally regulates MMTV expression.

(A) DAC induces transcriptional upregulation of *IFNB1* in MC38 cells. Expression was quantified by qRT-PCR. (B) DAC treatment increases IFN-β and IRF7 protein levels in 4T1 tumors. BALB/c mice were treated daily for 5 days and every other day thereafter. Protein abundance was analyzed by immunoblotting. Normalized band intensities are shown below the blots. (C) MMTV knockdown reduces IFN-β protein expression in 4T1 cells. Western blot analysis of KD1–KD3 knockdown lines compared with control. (D) Knockdown of *IFNB1* increases MMTV Env expression in 4T1 cells. Western blot showing reciprocal regulation of IFN-β and MMTV Env. (E) Recombinant IFN-α suppresses proliferation of *IFNB1*-deficient 4T1 cells. Cell proliferation of KD1 and KD2 lines was more sensitive to IFN-α than controls. (F) Effect of *IFNB1* knockdown and DAC treatment on 4T1 cell proliferation. Viable cell counts were determined by NucleoCounter. (G) *IFNB1* knockdown reduces sensitivity of 4T1 cells to DAC in vitro. Percent inhibition was calculated relative to untreated controls. (H) Tumor growth kinetics of control and *IFNB1* knockdown 4T1 tumors in BALB/c mice treated with PBS or DAC. Tumor volumes were measured longitudinally after inoculation. (I) Growth rate analysis of 4T1 tumors following *IFNB1* knockdown and DAC treatment. Pairwise comparisons included untreated and DAC-treated groups, as well as untreated tumors from control versus KD1.

Values represent medians with 95% confidence intervals. $n = 4$ for in vitro proliferation assays (A, E–G); $n = 6–7$ for control and KD1, and $n = 10$ for KD2 in in vivo studies (H–I). Abbreviations: DAC, decitabine; IFN, interferon; IFN-β, interferon beta; IFN-α, interferon alpha; IRF7, interferon regulatory factor 7; GAPDH, glyceraldehyde 3-phosphate dehydrogenase; MMTV, mouse mammary tumor virus; Env, envelope protein; KD, knockdown; PBS, phosphate-buffered saline; qRT-PCR, quantitative reverse transcription polymerase chain reaction.

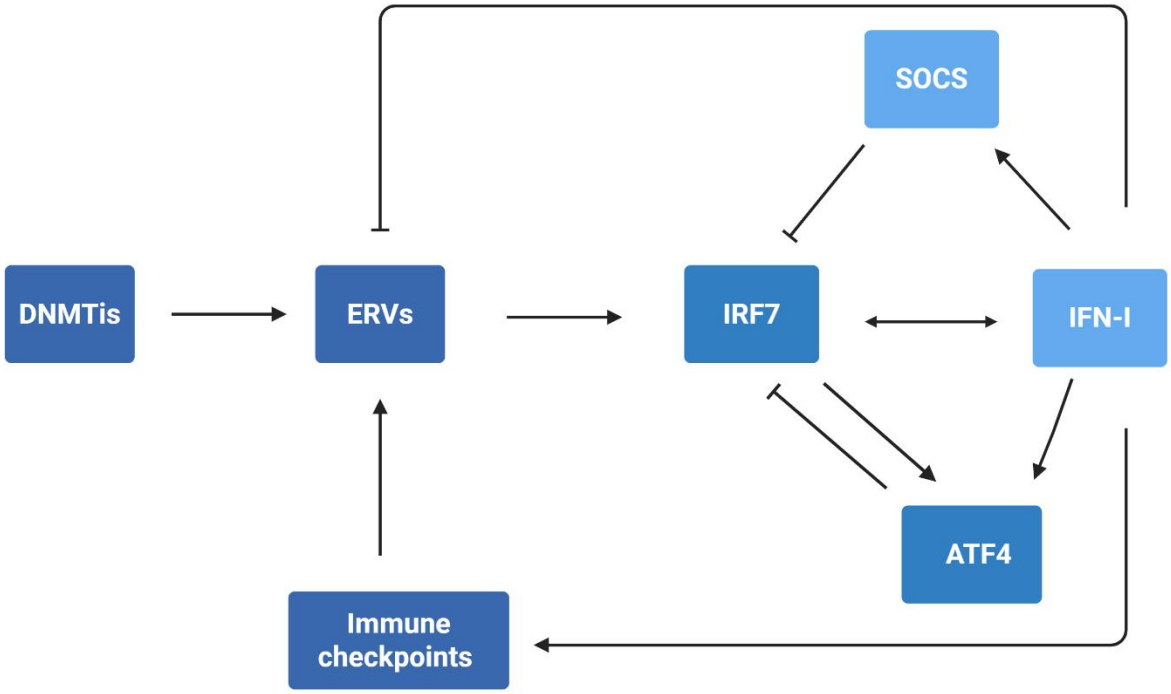

Figure 4. The interplay between DNMTis, ERVs, IFN-I, and immune checkpoints. DNMTis activate ERVs which, in turn, activate IRF7 and IFN-I. The latter two mutually stimulate each other. IFN-I inhibits both ERV expression and tumor growth. SOCS and ATF4 serve as mediators of negative feedback for the interferon system. Chronic expression of IFN-I activates immune checkpoints, leading to uncontrolled ERV expression and tumor growth. Abbreviations: DNMTis, DNA methyltransferase inhibitors; ERVs, endogenous retroviruses; IRF7, interferon regulatory factor 7; IFN-I, type I interferons; SOCS, suppressors of cytokine signaling; ATF4, activating transcription factor 4. [Created in BioRender. Liu, Y. (2025) https://BioRender.com/tx85roj]